

# Parameters Affecting the Rate and Product of Liquid Silicon Oxidation

Mari K. Næss · Jan Erik Olsen · Stefan Andersson ·  
Gabiella Tranell

Received: 25 June 2014 / Revised: 15 August 2014 / Published online: 6 September 2014  
© The Author(s) 2014. This article is published with open access at Springerlink.com

**Abstract** The oxidation of liquid silicon resulting in silica fume has been the subject of previous investigation due to its importance to occupational health in the silicon alloy production industry. Small-scale experiments and industrial measurements have been carried out in order to understand the mechanisms and kinetics of liquid silicon oxidation. Key questions as to the main factors and conditions determining the rate of fume formation in the industry, still remain. In this work the rate of active oxidation of liquid silicon was studied by experimental investigations in a 75 kW induction furnace, where oxidizing gas was introduced via a lance above the liquid silicon surface. The silica formed as a result of the reaction was collected and the silica fuming rate determined as a function of gas composition and gas flow velocity. The system was also modeled using computational fluid dynamics (CFD) and kinetic modeling. The flux of silica increases with increased gas velocity above the liquid surface, and was found to correlate well with mass transfer rates calculated from impinging jet theory. The size of the silica particles was also found to be dependent on the gas flow rate; smaller average particle size was obtained at higher flow rates. It was found that the most important factor for the silicon oxidation reaction rate is the velocity of the gas in vicinity of the silicon surface (i.e. the boundary layer thickness). The velocity is more important than the actual amount of oxygen delivered to the system per unit time, indicating that oxygen “efficiency” is not a strong function of oxygen concentration in the gas. Thus, the gas velocity is the rate determining parameter in determining the mass transport of oxygen to the silicon surface. Results from computational fluid dynamics simulations show that the gas flow was laminar in all experiments and that oxidation takes place within

---

M. K. Næss · G. Tranell (✉)  
Norwegian University of Science and Technology (NTNU), 7491 Trondheim, Norway  
e-mail: gabriella.tranell@ntnu.no

M. K. Næss · J. E. Olsen · S. Andersson  
SINTEF Materials and Chemistry, 7465 Trondheim, Norway

0.5 mm from the silicon surface. The results from the experiments and the CFD model were used to suggest a molecular mechanism of the active oxidation of liquid silicon.

**Keywords** Active oxidation · Kinetics · Liquid silicon · Diffuse emissions · Amorphous silica fume · CFD modeling · Kinetic modeling

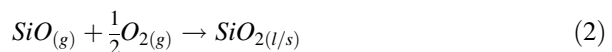
## Introduction

In recent years, the restrictions enforced by authorities on the working environment for operators in the Norwegian ferroalloy industry have become stricter. As a consequence, there has been increased attention to monitoring the fugitive emissions which have an impact on this environment and attempts to quantify the emissions have been made [1].

In a typical ferroalloy plant producing metallurgical grade silicon (MG-Si), there are significant fugitive emissions of fumed silica related to the tapping, refining and casting processes, and fume hoods are not always adequate or able to capture all fume.

In the production of metallurgical grade silicon the tapping and refining processes account for 40–80 % of all fugitive emissions from a silicon production site [2]. In the refining process, exposure of liquid silicon to air results in the formation of large amounts of condensed silica fume ( $\text{SiO}_2$ ). In earlier work [1, 3], the fume/fuming was characterized and quantified: it consists of spherical, amorphous silica particles with an average diameter of  $\sim 60$  nm. The flux of silica from the high-silicon alloy refining ladle, was found to be approximately 1 kg  $\text{SiO}_2$  per ton of Si produced, i.e. equivalent to 25 tons of silica per year for typical 25,000 ton annual production furnace [4].

The major mechanism behind the fume formation was also established; active oxidation of the liquid silicon surface. As such, the extent of oxidation is coupled to the available metal surface area exposed to the air. The silicon is first partially oxidized to SiO gas (Eq. 3) which escapes the surface and is subsequently further oxidized in a combustion reaction to become  $\text{SiO}_2$  fume (Eq. 4). The fume consists of small, amorphous spheres of glassy silica [1, 3, 5].



If the oxygen partial pressure in the bulk gas above a stagnant silicon surface is increased above a certain maximum pressure ( $6.1 \times 10^{-3}$  atm at 1,410 °C according to Wagner [5]), passivation of the surface will occur; a layer of oxide will form on the silicon surface, inhibiting further oxidation:



The rate of the *active* oxidation of liquid silicon (Eq. 1) was also recently investigated in small scale experiments, where a laminar flow of different Ar-O<sub>2</sub> mixtures was carried over a stagnant silicon surface. The reaction mechanism and reaction product found in the industry were reproduced, but not the rate of fume production or the oxidation conditions (oxygen partial pressure and a dynamic silicon surface) [3]. A comparison of the earlier industrial measurements and the small scale experiments, is shown in Fig. 1, with conditions applied and results for the flux of Si as SiO<sub>2</sub> tabulated in Table 1.

While the disagreement in order of magnitude in Si/SiO<sub>2</sub> flux per unit exposed Si area between industrial and small scale experiments may in part be explained by uncertainties in reaction area for industrial conditions [4], the key question of which main factors and conditions determine the rate of fume formation in the industry, still remain.

The molecular reaction mechanism for the active oxidation of liquid silicon is not yet fully understood, but it is generally accepted [6] that the chemical reaction is fast due to the high temperature and that the transport of reactant and/or product are the rate limiting steps. The diffusion of oxygen towards the silicon surface ( $J_{O_2}$ ), and SiO<sub>(g)</sub> away from the surface ( $J_{SiO}$ ) are linear according to Fick's law [7];

$$\frac{1}{2}J_{SiO} = J_{O_2} = \frac{k_{O_2}}{RT} p_{O_2}^\circ = \frac{1}{2} \frac{k_{SiO}}{RT} \cdot p_{SiO}^* \tag{4}$$

Here  $k_i$  is the mass transfer coefficient for species  $i$  [ $m\ s^{-1}$ ],  $R$  is the gas constant,  $T$  is the absolute temperature and the stoichiometric balance between SiO and O<sub>2</sub>

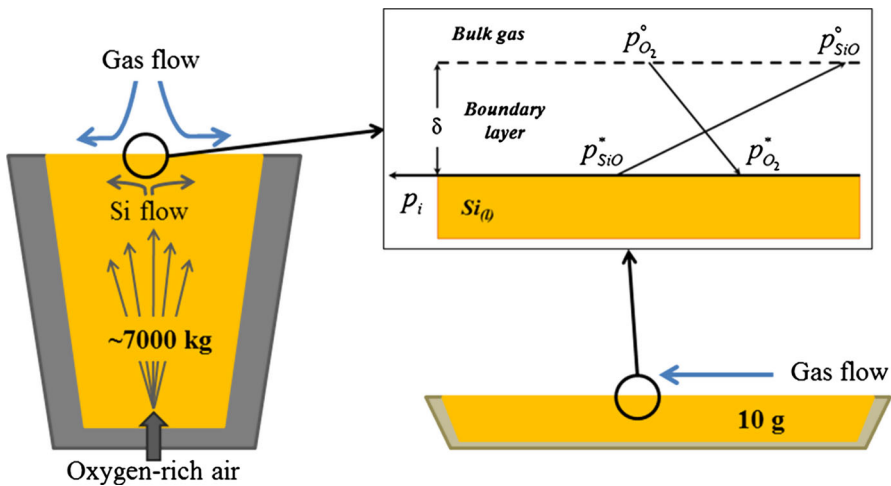


**Fig. 1** Comparison of the conditions in earlier industrial measurements of fume formation and small scale laboratory experiments. The mechanism for the oxidation, given in the *top right inset*, is the same for both cases; active oxidation [1, 3]

**Table 1** Comparison of the conditions and results from industrial measurements of fume formation and fundamental small scale experiments. [1, 3]

Industrial measurements	Small scale experiments
Turbulent, moving surface	Stagnant surface
Turbulent natural convection in air above silicon surface	Forced, laminar flow of Ar-O <sub>2</sub> above silicon surface
$p_{O_2}^o = 0.21$ atm	$p_{O_2}^o = 2 \times 10^{-3}$ atm
$J_{Si} = 0.018\text{--}0.037$ mol m <sup>-2</sup> s <sup>-1</sup>	$J_{Si} = 2.5 \times 10^{-4}\text{--}7.5 \times 10^{-4}$ mol m <sup>-2</sup> s <sup>-1</sup>

fluxes is recognized. In the classical flat plate theory for gas reacting at an interface (as illustrated in the inset in Fig. 1), the mass transfer coefficient is a function of the square root of the linear gas velocity in vicinity of the surface,  $\sqrt{v_g}$  [7]. However, in the theory for an *impinging laminar gas jet* reacting at a surface, the mass transfer coefficient is, according to Scholtz theory (1970) [8], a function of the linear gas velocity to the power of  $\frac{3}{4}$ ,  $v_g^{\frac{3}{4}}$ :

$$\text{Sh} = 0.5071 \text{Re}^{\frac{3}{4}} \cdot \left(\frac{x}{R}\right)^{-\frac{3}{4}} \cdot 0.1955 \text{Sc} \quad (5)$$

where

$$\text{Sh} = \frac{k_i l}{D}, \text{Re} = \frac{\rho v_g l}{\mu}, \text{Sc} = \frac{\mu}{\rho D} \quad (6)$$

Sh denotes Sherwood number, Re the Reynolds number and Sc the Schmidt number.  $x$  is the distance from the stagnation zone (in the center of the surface),  $R$  is radius of the jet nozzle,  $l$  is the characteristic length (in this case the nozzle diameter),  $D$  is the diffusion coefficient,  $\rho$  is the density,  $\mu$  is the viscosity and  $v_g$  is the linear gas velocity. Using this relation it is possible to relate the measured flux of silica to the linear gas velocity in the impinging jet system.

The overall objective of this work was to establish how external factors such as ambient flow rate and concentration of oxygen in the gas affect the rate of silica formation by active oxidation of a liquid silicon surface. In addition, fundamental insights into where and how the oxidation reactions take place on a molecular scale were sought. Methods applied to obtain this knowledge were experimental, computations fluid dynamics (CFD) and kinetic modelling.

## Experimental Procedures

### Laboratory Work

Experiments were performed in a 75 kW induction furnace from Inductotherm Europe Ltd. MG silicon was melted in a graphite crucible, and the typical sample batch was 1,750 g of refined metallurgical grade silicon (99 % Si). The crucible was

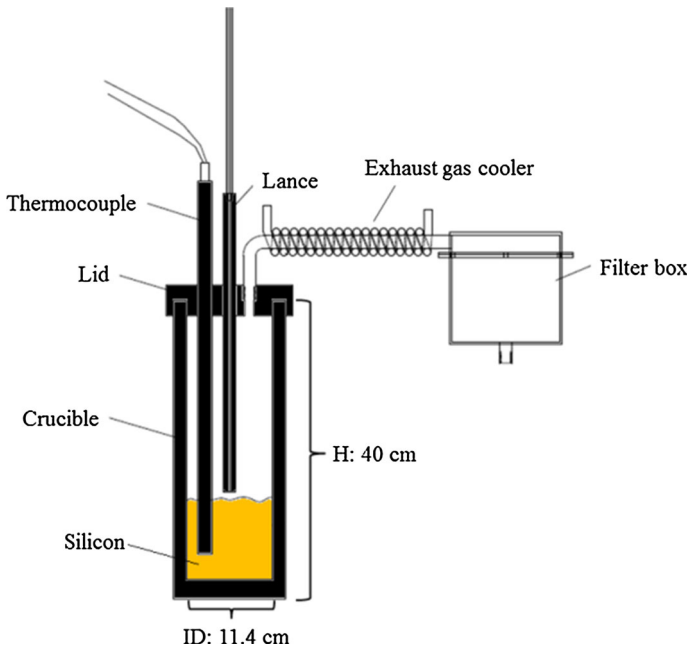


**Fig. 2** Sketch of experimental setup

covered with a specially designed lid with three holes; one for the graphite thermowell where an S-type thermocouple was placed, one for the graphite lance and one for the exhaust port with a cooler and a filter attached. The experimental setup is shown in Fig. 2. The filter used was an industrial filter of the type Gore Acid Resistant Fiberglass. The cooling system was applied due to the maximum working temperature of the filter of 280 °C.

The gas delivery lance was connected to a mass flow meter which was connected to synthetic air (99,9995 % purity). In order to avoid oxidation of the inside of the graphite lance, an alumina tube was placed inside the graphite tube. The inner diameter of the lance, ( $l$  in Eq. 6) was 5 mm for all experiments.

The silicon was heated to  $1,550 \pm 11$  °C, and kept at this temperature during the gas blowing. After the synthetic air was set to the desired flow rate, the lance was lowered so that the tip was situated 2.5 cm above the silicon melt surface. Experiments at 16, 21 and 26  $\text{m s}^{-1}$  gas velocity (at the lance exit) were held for 30 min, and the experiments at 5  $\text{m s}^{-1}$  gas velocity were held for 60 min.

Fifteen experiments were carried out in dry air. In addition, two parallel experiments with humid air were performed to mimic a rainy day by the Norwegian fjords, where most of the silicon plants are situated. The synthetic air was then bubbled through a water bath at 23.5 °C, obtaining a partial pressure of water of 0.03 atm. The humid air experiments were performed at 16  $\text{m s}^{-1}$  gas velocity at lance exit, and held for 20 min.

**Table 2** The experimental matrix with number of experiments performed at each condition is indicated. The diluted experiments are given with the proportional mixture of air:argon

Type of air	Linear gas velocity at lance tip, m s <sup>-1</sup>			
	5	16	21	26
Dry	2	2	2	2
Wet		2		
Diluted 1:4				2
Diluted 1:2		2		
Diluted 3:2				2

To establish the relationship between oxygen concentration/oxygen flow rate and oxidation rate, experiments with the same oxygen flow but in concentrated or diluted carrier gases, were performed. Three different dilutions were explored, two where the gas velocity was the same as in the 26 m s<sup>-1</sup> experiment, but with the same oxygen amount as in the 5 and 16 m s<sup>-1</sup> experiment, and one with the same gas velocity as the 16 m s<sup>-1</sup>, but with oxygen amount of the 5 m s<sup>-1</sup> experiment. The synthetic air was diluted 1:4, 1:2 and 3:2 with Ar. These experiments were held for 20 min. The experimental matrix is shown in Table 2, where the number of experiments at each flow rate and gas composition is indicated.

To monitor the amount of silica produced, all parts of the experimental equipment where silica deposited (mainly the cooler and the filter) were weighed before and after each experiment, and the weight gain was summed up to be the total amount of silica produced. The amount of silica in grams was used to calculate the average flux of SiO<sub>2</sub> in moles m<sup>-2</sup>s<sup>-1</sup>, assuming a flat silicon surface of 102 cm<sup>2</sup>.

Fume samples from the experiments were examined in a scanning electron microscope (SEM). The equipment used was a Zeiss Ultra 55 Limited Edition field emission microscope. The samples were held in place by a carbon tape in order to avoid charging, and the images were recorded at an acceleration voltage of 5 kV, with magnifications 2–50 k.

The specific surface area of the fume samples were measured with BET to find the average particle diameter. The samples were degassed over night at 250 °C under vacuum in a VacPrep 061 from Micromeretics, and analyzed with liquid nitrogen in a Tristar<sup>TM</sup>3000 from Micromeretics.

## Modelling

In order to evaluate the flow fields at the different gas velocities, CFD modeling was performed. CFD calculates the flow field from differential equations expressing conservation of mass and momentum. Conservation of atomic species and reaction schemes and kinetics may also be included to study reactive phenomena as previously demonstrated with a simplified reaction scheme [9]. In this study a more complete reaction scheme was implemented, in accordance with the latest results

**Table 3** Reactions and rate coefficients implemented in the CFD model

Reaction	A	n	$E$ [J/kmol]
I $\text{Si}_{(l)} + \frac{1}{2}\text{O}_{2(g)} \rightarrow \text{SiO}_{(g)}$	*	*	*
II $\text{SiO}_{(g)} + \text{O}_{2(g)} \leftrightarrow \text{SiO}_{2(g)} + \text{O}_{(g)}$	$1.0 \times 10^{10}$	0.0	$2.720 \times 10^7$
III $\text{SiO}_{(g)} + \text{O}_{(g)} + \text{M} \leftrightarrow \text{SiO}_{2(g)} + \text{M}$	$2.5 \times 10^9$	0.0	$1.828 \times 10^7$
IV $\text{SiO}_{2(g)} \rightarrow \text{SiO}_{2(s)}$	$5.0 \times 10^{10}$	0.5	0

\*not known, but available by model calibration

described in earlier publications [9, 10]. The reaction rates for the sub-reactions in the oxidation process are governed by the modified Arrhenius equation.

$$k_i = A_i T^n e^{-E_i/RT} \quad (7)$$

where  $k_i$  is the rate coefficient for reaction  $i$ ,  $T$  is temperature,  $A_i$  is pre-exponential factor,  $n$  is temperature exponent,  $E_i$  is activation energy and  $R$  is the universal gas constant. The reaction rates are listed in Table 3.

The rate coefficients of Reactions (II) and (III) in Table 3 were originally derived by Jachimowski and McLain [11] from semi-empirical model calculations and comparison with the analogous carbon reactions and subsequently successfully used in modelling combustion of silicon species by for instance Britten et al. [12] and Chagger et al. [13]. The coefficients for Reaction (IV) were estimated in this study by kinetic gas theory (see Appendix). The rate of Reaction (I) is unknown, but a quantitative estimate can be given by calibrating CFD results with experiments. These reaction rates are used as source and sinks in the transport equations for tracking of gas species.

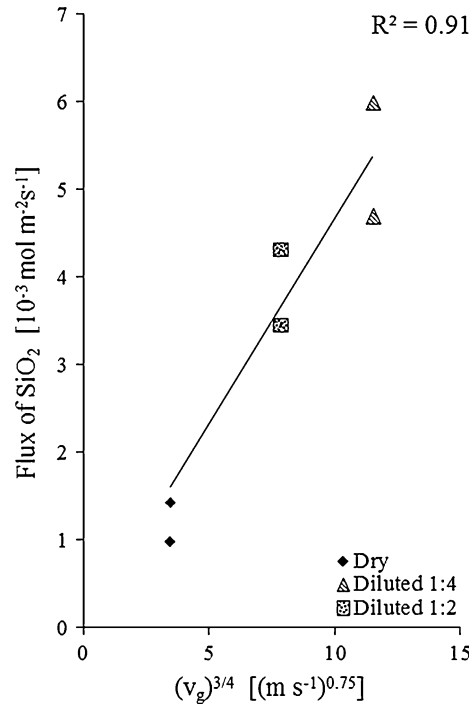
## Results and Discussion

### Rate of Fume Formation as a Function of Gas Velocity

The experimentally measured flux of  $\text{SiO}_2$  as a function of  $v_g^{\frac{1}{3}}$  is plotted in Fig. 3, where the linear dependency of the flux of  $\text{SiO}_2$  with  $v_g^{\frac{1}{3}}$  is illustrated with a regression line on the dry air experimental results. The fluxes were calculated from the surface area of the silicon, measured weight of silica produced and blowing time. Two parallels at each flow rate and gas composition were performed, and the variation between parallels was 3–37 %. When the flux was plotted in the same manner as a function of  $v_g^{\frac{1}{2}}$  in accordance with the flat plate theory, the regression line for the dry air points had an  $R^2$  value of 0.76, which is a bit lower than the impinging jet plot in Fig. 3.

The  $\text{SiO}_2$  fluxes measured in the present setup and plotted in Fig. 3 and given in full in Table 4, are in between those measured in the small scale laminar flow study and the turbulent surface industrial study. The experiment with humid air gave an absolute increase in the flux of 68 % as compared to dry air, thus water may have an

**Fig. 3** Measured flux of  $\text{SiO}_2$  as a function of  $v_g^{3/4}$  for three different flow rates with the same oxygen amount per time (Diamonds Exp. 1 and 2, Triangles Exp. 13 and 14, Squares Exp. 11 and 12)



effect in the fuming rate in industry. This phenomenon has also been observed for oxidation of aluminium by Wilson (2013) [14]. However, statistically, the flux is still within the experimental error, and when calculating the oxygen consumption (the ratio of amount of oxygen consumed to the amount of oxygen delivered), this was only increased from 4 % with dry air to 6 % with wet air. From these results we cannot with certainty conclude that humidity significantly affects the rate of fume formation when liquid silicon is actively oxidized in industry.

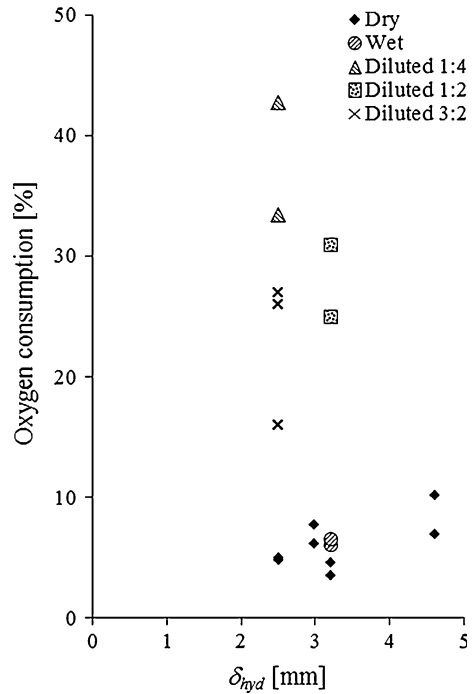
The CFD model was calibrated against the experiments performed at  $16 \text{ m s}^{-1}$  gas velocity to obtain kinetics of Reaction (I) (Table 3). Comparison with experiments at all other gas rates showed consistency between model and measurements. The CFD model showed that the flow was laminar in all experiments, and that there is a linear relation between the gas velocity at the lance tip and the gas velocity along the surface at all flow rates. An average radial gas velocity and average hydrodynamic boundary layer thickness were extracted from the CFD model. The consumption of available oxygen as a function of the average boundary layer thickness,  $\delta_{hyd}$ , is shown in Fig. 4. The gas velocity is inversely correlated with the hydrodynamic boundary layer thickness. The fact that the consumption of oxygen or “oxygen efficiency” decreases with increased gas flow rate tells us that the decrease in the boundary layer thickness is not proportional to the increase in amount of oxygen delivered per unit time. In fact, there is a linear decrease in the oxygen efficiency as the boundary layer thickness becomes thinner (Fig. 4). At  $5 \text{ m s}^{-1}$ , the flux of  $\text{SiO}_2$  was  $1.2 \times 10^{-3} \text{ mol m}^{-2} \text{ s}^{-1}$ , and at  $26 \text{ m s}^{-1}$



**Table 4** Specifications of each experiment (gas type, gas velocity ( $v_g$ ), moles of  $O_2$  per minute), Measured flux of  $SiO_2$ , oxygen consumption, modeled boundary layer thickness from the CFD model, measured average particles size from BET and calculated formation time for the average particle size

Exp #	Gas	$v_g$ , m/s	$P(O_2)$ , atm	Moles of $O_2$ per min, moles $min^{-1}$	Measured flux, $J_{SiO_2}$ , $\cdot 10^{-3}$ mol $m^{-2}s^{-1}$	Calculated $O_2$ used, %	$\delta_{hyp}$ from CFD, mm	Measured particle diameter (BET), nm	Calculated formation time, s
1	Dry air	5	0.21	0.009	0.98	7	4.6	91 ± 0.14	0.013
2	Dry air	5	0.21	0.009	1.43	10	4.6		
3	Dry air	16	0.21	0.026	1.48	4	3.2	63 ± 0.11	0.011
4	Dry air	16	0.21	0.026	1.93	5	3.2		
5	Dry air	21	0.21	0.034	3.50	6	3.0	72 ± 0.14	0.0091
6	Dry air	21	0.21	0.034	4.36	8	3.0		
7	Dry air	26	0.21	0.043	3.50	5	2.5	66 ± 0.15	0.010
8	Dry air	26	0.21	0.043	3.40	5	2.5		
9	Humid air	16	0.225	0.026	2.76	6	3.2	57 ± 0.10	0.0050
10	Humid air	16	0.225	0.026	2.98	7	3.2		
11	Air:Ar 1:4	26	0.042	0.009	5.99	43	2.5	40 ± 0.070	0.0019
12	Air:Ar 1:4	26	0.042	0.009	4.69	33	2.5		
13	Air:Ar 1:2	16	0.07	0.009	3.46	25	3.2	57 ± 0.13	0.0038
14	Air:Ar 1:2	16	0.07	0.009	4.31	31	3.2		
15	Air:Ar 3:2	26	0.126	0.026	6.55	16	2.5	55 ± 0.12	0.0026
16	Air:Ar 3:2	26	0.126	0.026	10.74	26	2.5		
17	Air:Ar 3:2	26	0.126	0.026	11.34	27	2.5		

**Fig. 4** The average oxygen consumption as a function of average hydrodynamic boundary layer thickness from CFD modeling,  $\delta_{hyd}$



it was  $3.5 \times 10^{-3} \text{ mol m}^{-2}\text{s}^{-1}$ . If the oxygen efficiency was the same, the flux would have to be fivefold, however the measured increase in flux was only a factor of 2.9, which reflects the decrease in oxygen consumption from 9 % at  $5 \text{ m s}^{-1}$  to 5 % at  $26 \text{ m s}^{-1}$ . The explanation for this is likely that the transport of oxygen towards the silicon surface is too slow to exploit the increased oxygen amount, and thus less oxygen is consumed.

The experiments performed with 1:4 air:Ar gave a large increase in the flux compared to the experiment with the same amount of oxygen being introduced per unit time at  $5 \text{ m s}^{-1}$ . The oxygen consumption went from an average of 9 % at  $5 \text{ m s}^{-1}$  air, to 38 % at  $26 \text{ m s}^{-1}$  in the 1:4 air-Ar mixture. This indicates that the gas flow rate, and thus the boundary layer thickness, is more important to increase the flux of silica, than the oxygen partial pressure. The transport of oxygen from the bulk gas to the silicon surface is the factor limiting the rate of oxidation of the silicon. This is also reflected in the fact that there is no accumulation of  $\text{SiO}_{(g)}$  close to the surface as the gas velocity increase. An experimental  $p_{\text{SiO}}$  was calculated with the mass transfer coefficient derived from the impinging jet theory, and it was found that the partial pressure of  $\text{SiO}_{(g)}$  was principally the same for all gas flow rates (0.0037–0.0068 atm), with only 25 % standard deviation. This implies that the transport of  $\text{SiO}_{(g)}$  away from the surface is not rate limiting, as there is no accumulation of  $\text{SiO}_{(g)}$  at the surface with a higher rate of oxygen coming in. The sole factor limiting the oxidation rate is thus the transport of oxygen to the silicon surface. Comparing the diffusion coefficients (calculated using the method

described by Bird, Stewart and Lightfoot [15], see [4] for more elaborated description and derivation of the calculation) of SiO ( $D_{SiO-N_2} = 3.9 \times 10^{-4} \text{ m}^2\text{s}^{-1}$  at 1,550 °C) and O<sub>2</sub> ( $D_{O_2-N_2} = 4.7 \times 10^{-4} \text{ m}^2\text{s}^{-1}$  at 1,550 °C) shows that the transport of SiO<sub>(g)</sub> should have been slightly slower than that oxygen, however, when we take into account that the SiO gas is readily consumed in the combustion to become SiO<sub>2(g)</sub> and later grow into silica particles, the transport of SiO<sub>(g)</sub> will most probably be enhanced.

One of the outputs from the CFD model was the concentration profiles for all species included in the model. Plotting these concentration profiles it was found that the concentration boundary layer thickness for O<sub>2(g)</sub> and SiO<sub>(g)</sub> are different by one order of magnitude.

In Fig. 5, the concentration profiles for O<sub>2(g)</sub> and SiO<sub>(g)</sub> at the highest and lowest experimental gas velocities are given. From this it can be clearly seen that the SiO<sub>(g)</sub> boundary layer thickness is similar and <0.5 mm at all gas flow rates, but that the oxygen boundary layer thickness changes radically with gas flow. This supports the findings in the experimental results that the oxygen transport to the silicon surface is the sole factor determining the rate of fume formation.

Using the mass transfer coefficient for oxygen found by Scholtz' equation (Eq. 5–6) to calculate the flux of Si with Fick's law (Eq. 4), and a sticking coefficient of 0.01 (probability of O<sub>2</sub> to stick to the Si surface) as proposed by Lander and Morrison (1962) [16], the fluxes obtained by this theoretical calculation are in the same order of magnitude as the measured fluxes, as can be seen in Table 5. The sticking coefficient was found by measuring pressure drop due to consumption of oxygen in the reaction with solid silicon at 875 °C. Lander and Morrison found that the sticking coefficient was not strongly temperature dependent, and thus concluded that the activation energy for active oxidation was low.

The similarity of measured and theoretically calculated flux of silicon signifies that the theoretical calculation of a mass transfer coefficient for oxygen may be applied, assuming that the sticking coefficient is correct.

### Reaction Product and Fume Formation Mechanism

The oxidation reaction product was confirmed to be the same as the silica found in industry [1] and small scale experiments [3]: small, spherical particles of amorphous silica, shown in Fig. 6. This confirms that the experiments were performed in the active oxidation regime. The BET analysis showed that the particles formed at a lower gas flow rate had a larger average particle diameter (91 nm) than the silica formed at higher gas flow rates (66 nm). The average particle sizes are presented in Table 5. The explanation for this significantly different particle size likely lies in Ulrich et al.'s (1977) [17] theory of silica particle growth: the retention time for nucleated SiO<sub>2</sub> particles in the hot gas is longer at low flow rate, thus the particles have the time to grow larger. The average particle sizes are similar to that found in silica samples from the refining process in industry, which had an average particle size of 56–66 nm.

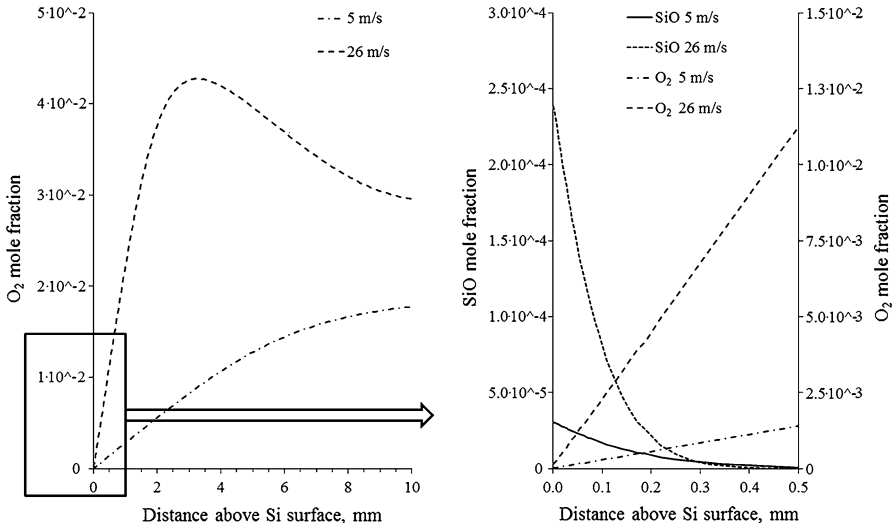
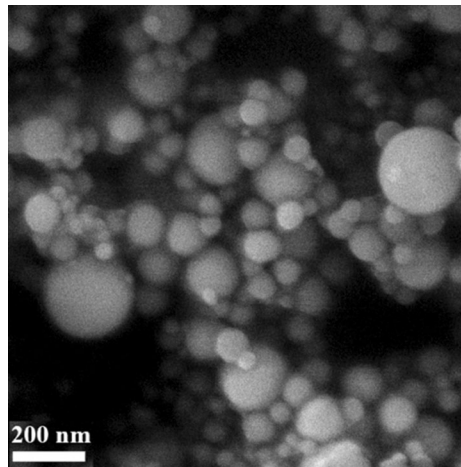


**Fig. 5** Concentration profile of O<sub>2</sub> and SiO at the highest and lowest gas flow rates. Note the different y-scales in the *right graph*

**Table 5** Comparison of measured flux of Si and theoretical flux of Si, calculated with mass transfer coefficient from laminar impinging jet theory, and using a sticking coefficient of 0.01

Gas velocity at nozzle exit	5 m/s	16 m/s	21 m/s	26 m/s
Measured $J_{SiO_2}$ , $10^{-3} \text{ mol m}^{-2}\text{s}^{-1}$	1.2	1.7	3.9	3.5
Theoretical $J_{SiO_2}$ , $10^{-3} \text{ mol m}^{-2}\text{s}^{-1}$	1.0	2.3	2.9	3.4

**Fig. 6** SEM image of the silica collected in the filter



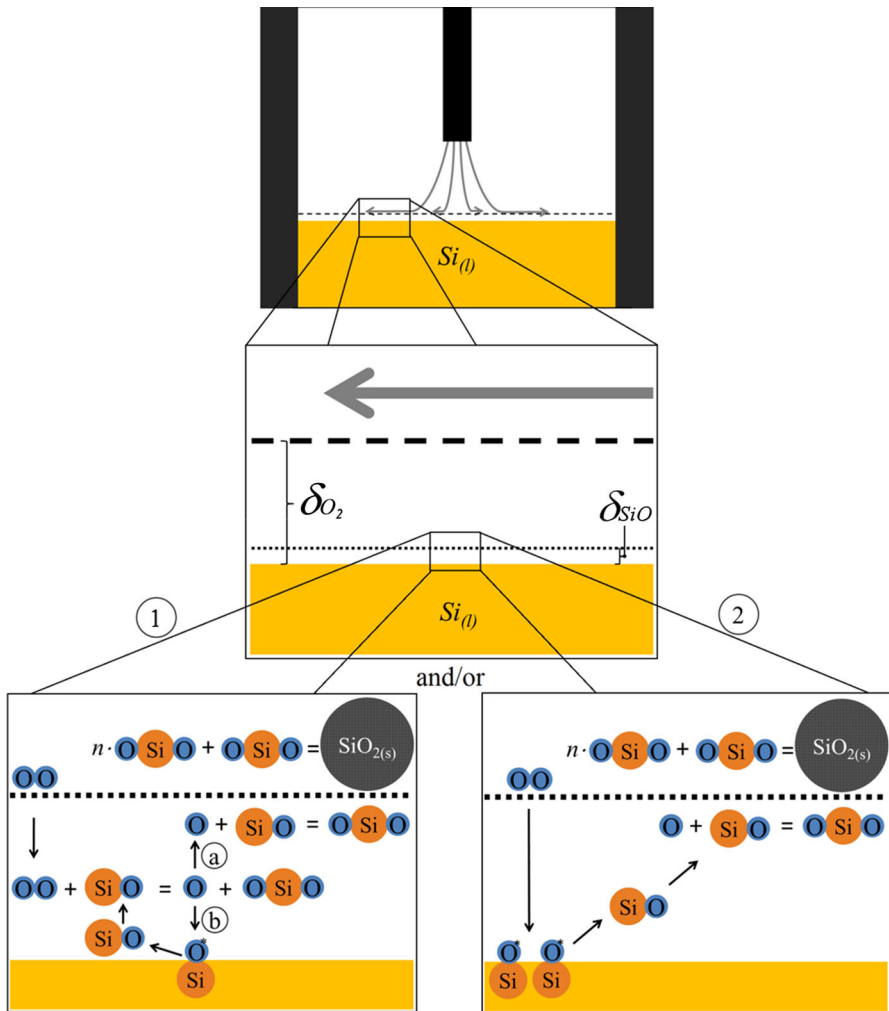


**Fig. 7** Sketch of suggested molecular mechanism for the active oxidation of liquid silicon. The boundary layer of  $\text{SiO}_{(g)}$  is one order of magnitude thinner than the  $\text{O}_{2(g)}$  boundary layer. The gas velocity will affect the  $\text{O}_{2(g)}$  boundary layer, but not the  $\text{SiO}_{(g)}$  boundary layer. When the oxygen travels through the  $\text{SiO}_{(g)}$  boundary layer, there are two possible paths: (1) it meets an outgoing  $\text{SiO}_{(g)}$  molecule and reacts to become an  $\text{SiO}_{2(g)}$  molecule and an  $\text{O}^{\cdot}$  radical, which further will (a) react with the Si surface and make a new  $\text{SiO}_{(g)}$  molecule, or (b) react with a  $\text{SiO}_{(g)}$  molecule to form more  $\text{SiO}_{2(g)}$ . (2) it reacts directly with the  $\text{Si}_{(l)}$  surface to form two  $\text{SiO}_{(g)}$  molecules which are oxidized to  $\text{SiO}_{2(g)}$

The average particle size was used to calculate a theoretical “formation time”, using Ulrich et al.’s method (for elaborated derivation, see Ref. [4]). By formation time, we mean the time it takes from the  $\text{SiO}_{2(g)}$  molecule meets another  $\text{SiO}_{2(g)}$  molecule to make a dimer( $\text{SiO}_2$ )<sub>2</sub>, until the particle has grown to the measured average particle size. The calculated formation times are given in Table 4, together with the average hydrodynamic boundary layer thickness found by CFD modeling.

Using the calculated formation time of the particles and the mass transfer coefficient for  $\text{SiO}_{2(\text{g})}$  found by Scholtz' method (Eq. 5–6), the distance traveled by the particle during formation was calculated. Comparing this distance to the concentration boundary layer thicknesses of  $\text{SiO}_{(\text{g})}$  and  $\text{O}_2$  from the CFD modeling (Fig. 5), it was found that the silica fume is formed mainly outside the  $\text{SiO}_{(\text{g})}$  boundary layer for all flow rates except  $5 \text{ m s}^{-1}$ , but inside the  $\text{O}_2$  boundary layer for all flow rates. Based on these calculations, a suggested mechanism for the surface oxidation and subsequent fume formation is shown in Fig. 7. At  $26 \text{ m s}^{-1}$ , the average oxygen boundary layer thickness is 3.25 mm, which is one order of magnitude larger than the  $\text{SiO}_{(\text{g})}$  boundary layer of  $<0.5 \text{ mm}$ . This is illustrated in the sketch in Fig. 7. Inside the  $\text{SiO}_{(\text{g})}$  boundary layer there are two possible paths for the oxygen molecule coming in during active oxidation:

- (1) It meets an outgoing  $\text{SiO}_{(\text{g})}$  molecule and reacts to become an  $\text{SiO}_{2(\text{g})}$  molecule and an  $\text{O}^*$  radical, which further will (a) react with the Si surface and make a new  $\text{SiO}_{(\text{g})}$  molecule, or (b) react with a  $\text{SiO}_{(\text{g})}$  molecule to form more  $\text{SiO}_{2(\text{g})}$ .
- (2) It reacts directly with the  $\text{Si}_{(\text{l})}$  surface to form two  $\text{SiO}_{(\text{g})}$  molecules which are oxidized to  $\text{SiO}_{2(\text{g})}$ . Eventually, all  $\text{SiO}_{(\text{g})}$  will react with oxygen to become  $\text{SiO}_{2(\text{g})}$  which will nucleate, condensate and grow to become a  $\text{SiO}_{2(\text{s})}$  particle of measured diameter, somewhere outside the  $\text{SiO}_{(\text{g})}$  boundary layer, but within the  $\text{O}_{2(\text{g})}$  boundary layer.

From empirical observations done by workers at the plant, there is an increased amount of fume formed during cold weather. This supports our results regarding the increased fume formation with increased gas flow rate above the silicon surface, because cold weather means a larger temperature difference between the bulk gas in the plant hall and the silicon surface, and thus an increased buoyancy effect and larger gas velocity close to the silicon surface. In the current study, the potential cooling effect of a higher gas flow rate could not be registered by a thermocouple held above the melt surface and hence not considered a factor influencing the oxidation rate.

## Conclusions

In this work, active oxidation of liquid silicon was studied, and the external factors affecting the rate of silica formation were investigated; ambient gas flow rate, oxygen partial pressure in the gas. The situation for fume formation found in the industry was mimicked in terms of having a moving silicon surface and an impinging jet of reaction gas: synthetic air was blown towards the silicon surface through a lance. It was found that the measured experimental flux of silica fits with Scholtz theory on impinging laminar jets, and that the transport of oxygen to the silicon surface is the sole factor determining the rate of fume formation. The oxygen "efficiency", i.e. the fraction oxygen consumed in silicon oxidation, does not increase significantly with a higher concentration of oxygen in the gas flow.

Humidity in the gas ( $p_{H_2O(g)} = 0.03$  atm) showed a small, statistically non-significant increase in the rate of fume formation.

Calculations of an “experimental SiO partial pressure” at the surface showed that here is no accumulation of SiO at the surface with increased oxygen flux to the surface. Using the measured average particle size of the silica formed, Scholtz’s impinging jet theory for mass transfer and Ulrich’s theory for silica condensation, a formation time for the particles was estimated. The calculated formation time of the particles indicates that the silica particle growth occurs inside the oxygen concentration boundary layer for all flow rates investigated. However, the convection in the gas phase will most probably carry the particles away from the vicinity of the surface, and thus the presence of particles in the boundary layer will have minor effect on the diffusion of oxygen towards the silicon surface.

Results from CFD simulations show that the flow is laminar in controlled experiments and that the reaction boundary layer is very thin. Oxidation takes place within 0.5 mm from the metal surface.

As illustrated in the suggested molecular reaction mechanism, flow conditions above the silicon during industrial silicon refining will contribute significantly to the silica fuming rate. To reduce fuming, low flows/low temperature gradients should be aimed for.

**Acknowledgments** This work was funded by the Norwegian Research Council and FFF (The Norwegian Ferroalloy Producers Research Association) through the FUME project (Fugitive Emissions of Materials and Energy). We would like to express our appreciation to Elkem Thamshavn for providing silicon for the experiments.

**Open Access** This article is distributed under the terms of the Creative Commons Attribution License which permits any use, distribution, and reproduction in any medium, provided the original author(s) and the source are credited.

## Appendix: Kinetic Modeling of Condensation of SiO<sub>2</sub>

Upon formation of molecular SiO<sub>2</sub>, or SiO<sub>2</sub> *monomers* in the gas phase, SiO<sub>2</sub> will rapidly condense to form liquid and subsequently solid particles, since gas phase SiO<sub>2</sub> is a metastable phase at all relevant temperatures. In order to estimate the rate at which gas phase SiO<sub>2</sub> is transformed into the liquid/solid (particulate) phase, we introduce a parameter called *solidity*,  $s$ . It is defined as.

$$s = \left( \frac{N - 1}{N_{solid}} \right)^l \quad (8)$$

where  $N$  is the number of SiO<sub>2</sub> units,  $N_{solid}$  is the minimum number of SiO<sub>2</sub> units for the particle to thermodynamically be considered as solid state, and  $l$  gives the typical functional behavior of the heat of formation going from the gas to the solid state values. With growing particle size,  $s$  will increase from 0 (gas) to 1 (solid). The parameter  $N_{solid}$  can be defined as the typical particle size where the heat of formation of the particle is (almost) the same as the solid state. If  $s$  is used to describe

the typical phase of the system, then the effective heat of formation of  $\text{SiO}_2$ ,  $\Delta H_{\text{eff}}$ , will change as.

$$\Delta H_{\text{eff}} = (1 - s)\Delta H_{\text{gas}} + s\Delta H_{\text{solid}} \quad (9)$$

thus giving a smooth transition from the gas phase to the solid state, with  $\Delta H_{\text{gas}}$  and  $\Delta H_{\text{solid}}$  being the heats of formation of the gas-phase and solid  $\text{SiO}_2$ , respectively. The parameters for this equation were taken from a paper by Catlow et al. [18], where they performed density functional theory (DFT) calculations on increasing sizes of  $\text{SiO}_2$  clusters,  $(\text{SiO}_2)_N$ , from  $(\text{SiO}_2)_1$  to  $(\text{SiO}_2)_{27}$ . They found that from  $N = 13$  and up, the binding energy,  $E_b$ , follows an  $N^{-1/3}$  dependence. The binding energy is here defined as.

$$E_b = \frac{E_N}{N} - E_\infty \quad (10)$$

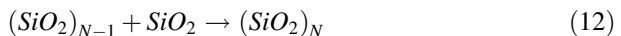
where  $E_\infty$  is the energy of bulk alpha-quartz per  $\text{SiO}_2$  unit. By extrapolating to larger  $N$  it was found that energetically a  $\text{SiO}_2$  particle of size  $N = 7,000$  would thermodynamically exhibit solid state behavior. A particle of this size would have a diameter of 8 nm if it is spherical and has the density of quartz. Obviously, in reality the particles can grow much larger than this, but for simulating the thermodynamics of  $\text{SiO}_2$  particle formation it is practical to set  $N_{\text{solid}} = 7,000$ . Considering the  $N^{-1/3}$  scaling of the binding energy, it seems reasonable to assume that  $l = 1/3$ . This gives the final expression for the solidity parameter as.

$$s = \left( \frac{N - 1}{7000} \right)^{\frac{1}{3}} \quad (11)$$

To estimate the growth rate of  $\text{SiO}_2$  particles a few assumptions were made:

1. Growth will only be determined by the addition of  $\text{SiO}_2$  monomers to  $\text{SiO}_2$  particles of any size.
2. The addition reaction is irreversible, i.e. evaporation is not possible.
3. Every collision between  $\text{SiO}_2$  and  $(\text{SiO}_2)_{N-1}$  gives  $(\text{SiO}_2)_N$  as products.
4. The formed particles are considered to be spherical.
5. Interactions between  $\text{SiO}_2$  and  $(\text{SiO}_2)_{N-1}$  units are treated as hard-sphere potentials.
6. The concentration of  $\text{SiO}_2$  monomers is constant.

Assumption 1 gives the reaction as



This simplified reaction scheme, which neglects addition of  $(\text{SiO}_2)_2$ ,  $(\text{SiO}_2)_3$ , etc. to larger particles, is justified by considering that the concentration of  $\text{SiO}_2$  monomers will be much higher than that of  $(\text{SiO}_2)_N$  of any size  $N > 1$ , in the regions where  $\text{SiO}_2$  is produced from  $\text{SiO}$ . The assumptions 2 and 3 are realistic considering



that binding between  $\text{SiO}_2$  units is quite strong [18]. This means that every collision between  $\text{SiO}_2$  and  $(\text{SiO}_2)_{N-1}$  is reactive. Regarding assumption 4 and 5, the very smallest particles will not be spherical, and  $\text{SiO}_2$  and  $(\text{SiO}_2)_{N-1}$  will experience an attractive interaction at longer distances than the typical particle diameter. A hard-sphere potential neglects these interactions, and should underestimate the collision rate somewhat, but at high temperatures this is not a determining factor for the kinetics. As for assumption 6, it is reasonable to assume constant  $\text{SiO}_2$  monomer concentration under steady-state conditions. A similar scheme was used by Lindackers et al. [19].

Given the above assumptions the rate for the formation of  $(\text{SiO}_2)_N$  can be calculated from hard-sphere collision theory [20], assuming each collision to be reactive as argued above. The expression is.

$$\frac{d}{dt} [(\text{SiO}_2)_N] = k_{\text{coll}} [\text{SiO}_2] [(\text{SiO}_2)_{N-1}] \quad (13)$$

where the collision rate constant is defined as

$$k_{\text{coll}} = \sigma \left( \frac{8k_B T}{\pi \mu} \right)^{\frac{1}{2}} N_A^2 \quad (14)$$

Here  $k_B$  is the Boltzmann constant,  $N_A$  is the Avogadro number,  $\mu$  is the reduced mass of collision partners A and B, with masses  $m_A$  and  $m_B$ :

$$\mu = \left( \frac{m_A m_B}{m_A + m_B} \right) \quad (15)$$

and  $\sigma$  is the collision cross section defined as

$$\sigma = \pi d^2 \quad (16)$$

with

$$d = \frac{1}{2} (d_A + d_B) \quad (17)$$

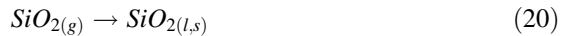
where  $d_A$  and  $d_B$  are the diameters of particles A and B, respectively. Considering that the concentration of  $\text{SiO}_2$  monomers is assumed to be constant the rate expression can be written

$$\frac{d}{dt} [(\text{SiO}_2)_N] = k_{\text{coll,eff}} [(\text{SiO}_2)_{N-1}] \quad (18)$$

with

$$k_{\text{coll,eff}} = k_{\text{coll}} (\text{SiO}_2) \quad (19)$$

To estimate the rate of the condensation of  $\text{SiO}_2$  as a first-order reaction:



it seems that the ideal way of expressing this is as the rate of change of the solidity parameter.

By numerically solving for the growth of  $\text{SiO}_2$  particles according to Eqs. (12–18), the rate constant of particle formation has been estimated according to.

$$k_{\text{particle}} = \tau_{\text{particle}}^{-1} \quad (21)$$

where  $\tau_{\text{particle}}$  is the time for  $(1-s)$  to grow to  $1/e$ , i.e., about 0.368. This is justified by the formulation of the reaction as a first-order reaction [Eq. (20)]. Under steady state conditions the reaction does behave as a true first-order reaction. The analysis gives the temperature dependent rate constant.

$$k_{\text{particle}} = 5 \cdot 10^{10} T^{\frac{1}{3}} s^{-1} \quad (22)$$

indicating that particle growth will increase with increasing temperatures. By using the density of amorphous silica ( $2.2 \text{ g cm}^{-3}$ ) to define the diameters of the particles, the rate constant becomes  $6 \times 10^{10} T^{1/2} s^{-1}$ , i.e. about 20 % higher than using the density of quartz. This is deemed to be an insignificant difference given the approximations in the model.

## References

1. M. K. Næss, G. Tranell, J. E. Olsen, N. E. Kamfjord and K. Tang, Mechanisms and Kinetics of Liquid Silicon Oxidation During Industrial Refining. *Oxidation of Metals* **78**, 2012 (239–251).
2. N.E. Kamfjord, *Mass and energy balances of the silicon process—Improved emission standards*, PhD. (Department of Materials Science and Engineering, Norwegian University of Science and Technology, Trondheim., 2012).
3. M. K. Næss, D. J. Young, J. Zhang, J. E. Olsen and G. Tranell, Active Oxidation of Liquid Silicon: Experimental Investigation of Kinetics. *Oxidation of Metals* **78**, 2012 (363–376).
4. M.K.Næss, *Mechanisms and kinetics of liquid silicon oxidation*, PhD thesis. (Department of Materials Science and Engineering, Norwegian University of Science and Technology (NTNU), Trondheim, 2013).
5. C. Wagner, Passivity during the oxidation of silicon at elevated temperatures. *Journal of Applied Physics* **29**, 1958 (1295–1297).
6. M. Ratto, E. Ricci, E. Arato and P. Costa, Oxidation of metals with highly reactive vapors: Extension of Wagner theory. *Metallurgical and Materials Transactions B* **32**, 2001 (903–911).
7. J. W. Hinze and H. C. Graham, The active oxidation of Si and SiC in the viscous gas-flow regime. *Journal of the Electrochemical Society: Solid State Science and Technology* **123**, (7), 1976 (1066–1073).
8. M. T. Scholtz and O. Trass, Mass transfer in an impinging jet. Part 2: Boundary layer flow mass transfer. *American Institute of Chemical Engineers Journal* **16**, 1970 (90–96).
9. J. E. Olsen, M. Næss and G. Tranell, *Understanding fuming during metal refining by CFD*, in *TMS Annual Meeting & Exhibition March 3–7, 2012: Orlando, (FL, USA, 2012)*.
10. J.E. Olsen, M. Næss, G. Tranell, , *CFD modeling of silica fume formation during refining of silicon metal*, in *8th International Conference on CFD in Oil & Gas, Metallurgical and Process Industries, (SINTEF/NTNU, Trondheim, 2011)*.
11. C.J. Jachimowski and A.G. McLain. *A chemical kinetic mechanism for the ignition of silane/hydrogen mixtures*, in *NASA Technical Paper 2129*. (Langley Research Center, National Aeronautics and Space Administration (NASA): Hampton, 1983).

12. J.A. Britten, J. Tong, and C.K. Westbrook, *A numerical study of silane combustion*. vol. 23, Twenty-Third Symposium (International) on Combustion/The Combustion Institute 1990, p. 195–202.
13. H.K. Chagger, D. Hainsworth, P.M. Patterson, M. Pourkashanian, and A. Williams. *The formation of SiO<sub>2</sub> from hexamethyldisiloxane combustion in counterflow methane-air flames*. vol. 26 (Twenty-Sixth Symposium (International) on Combustion/The Combustion Institute, 1996) p. 1859–1865.
14. S. Wilson. *Oxidation of Manganese-Containing Aluminium Alloys: Oxidation of Molten Mn-containing Al Alloys in Various Atmospheres*, (Master thesis, Department of Materials Science and Engineering, Norwegian University of Science and Technology (NTNU), Trondheim, 2013).
15. R.B. Bird, W.E. Stewart and E.N. Lightfoot, *Transport Phenomena*, 2nd edn. (Wiley Inc., 2002).
16. J. J. Lander and J. Morrison, Low voltage electron diffraction study of the oxidation and reduction of silicon. *Journal of Applied Physics* **33**, 1962 (2089–2092).
17. G. D. Ulrich and N. S. Surbramanian, Particle growth in flames III: Coalescence as a rate-controlling process. *Combustion Science and Technology* **17**, 1977 (119–126).
18. C. R. A. Catlow, S. T. Bromley, S. Hamad, M. Mora-Fonz, A. A. Sokol and S. M. Woodley, Modelling nano-clusters and nucleation. *Physical Chemistry Chemical Physics* **12**, (4), 2010 (786–811).
19. D. Lindackers, M. G. D. Strecker, P. Roth, C. Janzen and S. E. Pratsinis, Formation and Growth of SiO<sub>2</sub> Particles in Low Pressure H<sub>2</sub>/O<sub>2</sub>/Ar Flames Doped with SiH<sub>4</sub>. *Combustion Science and Technology* **123**, 1997 (287–315).
20. P.W. Atkins, *Physical Chemistry*, 4th edn. (Oxford University Press, 1990).